Electromagnetically Induced Transparency in a Diamond Spin Ensemble Enables All-Optical Electromagnetic Field Sensing

V. M. Acosta, K. Jensen, C. Santori, D. Budker, and R. G. Beausoleil

Electromagnetically-induced transparency in a diamond spin ensemble enables all-optical electromagnetic field sensing

V. M. Acosta,[1, *] K. Jensen,[2, †] C. Santori,[1] D. Budker,[2] and R. G. Beausoleil[1]

[1]*Hewlett-Packard Laboratories, 1501 Page Mill Rd., Palo Alto, CA 94304*
[2]*Department of Physics, University of California-Berkeley, Berkeley CA 94720*

We use electromagnetically-induced transparency (EIT) to probe the narrow electron-spin resonance of nitrogen-vacancy centers in diamond. Working with a multi-pass diamond chip at temperatures 6-30 K, the zero-phonon absorption line (637 nm) exhibits an optical depth of 6 and inhomogenous linewidth of $\sim$30 GHz full-width-at-half-maximum (FWHM). Simultaneous optical excitation at two frequencies separated by the ground-state zero-field splitting (2.88 GHz), reveals EIT resonances with a contrast exceeding 6% and FWHM down to 0.4 MHz. The resonances provide an all-optical probe of external electric and magnetic fields with a projected photon-shot-noise-limited sensitivity of 0.2 V/cm/$\sqrt{\text{Hz}}$ and 0.1 nT/$\sqrt{\text{Hz}}$, respectively. Operation of a prototype diamond-EIT magnetometer measures a noise floor of $\lesssim$1 nT/$\sqrt{\text{Hz}}$ for frequencies above 10 Hz and Allan deviation of 1.3$\pm$1.1 nT for 100 s intervals. The results demonstrate the potential of diamond-EIT devices for applications ranging from quantum-optical memory to precision measurement and tests of fundamental physics.

Electromagnetically-induced transparency (EIT) is an optical coherence effect which provides exquisite control over the absorption and dispersion in atomic media. In atoms with two coherent ground-state levels that can be optically excited to the same excited state (a "Λ system"), EIT results in ultra-narrow transmissive spectral features, with resonance quality factors exceeding 10^{12} [1–4] and more than 10^7 reduction in optical group velocity [2, 5]. Numerous EIT-based applications are being pursued, including precision measurement [6–9], few-photon nonlinear optics [10–13], optical buffers [14–16], and quantum optical memories [17–19].

Critical to EIT-based applications is the simultaneous presence of substantial atomic absorption and long-lived ground-state coherence [20]. This has motivated the use of atomic gases, where high optical depth ($\gg$1) and long coherence times ($\gg$1 ms) can be simultaneously realized [17, 19]. However, a solid-state approach is desirable for compatibility with large-scale fabrication processes. EIT in various rare-earth doped crystals has been observed [21–23], and there has been substantial progress towards applications in quantum information. However, one drawback of many rare-earth-doped systems is weak optical transitions [17, 18].

Ensembles of nitrogen-vacancy (NV) centers in diamond may provide an ideal compromise, owing to the relatively strong NV-light coupling [24, 25], which can be enhanced using optical microcavities [26–29], and long ensemble spin coherence time ($\gg$100 ms using decoupling techniques [30]) at temperatures $T\lesssim$100 K [31, 32]. EIT in diamond was observed before [33], but there the use of a high-defect-density diamond and the necessity of a large magnetic field ($\sim$0.1 T) limited the range of possible applications. More recent studies showed that Λ systems can be realized near zero magnetic field [34–38].

In this Letter, we report EIT with low-defect-density diamond at zero magnetic field. Using electron-irradiation and annealing techniques [39] to enhance the NV absorption coefficient, α, and a multi-pass diamond chip to increase the optical path length, L, we realize optical depth, $\alpha L > 1$, and coherence time, $T_2^* > 1$ μs. EIT provides a means of probing the NV ground-state spin resonances without microwave irradiation, and we show that high-sensitivity, all-optical electric and magnetic field sensing is possible even in the presence of large bias electric fields. These are desirable features for cryogenic applications such as fundamental physics experiments [40, 41] and studies of novel superconductors [42]. Our results are well-described by a model for EIT in inhomogenously-broadened media and can be extended to applications in nonlinear optics and quantum information.

The apparatus is depicted in Fig. 1(a). Light (637 nm) from an external-cavity diode laser (ECDL) was passed through an electro-optic phase modulator (EOM), producing sidebands with a tunable sideband-carrier detuning near 2.88 GHz. The EOM output was combined with a green repump beam (532 nm), necessary to reverse optical bleaching [33, 34, 43]. The light beam then traveled 8 times through a multi-pass diamond chip housed in a continuous-flow liquid-helium cryostat. The transmitted light was spectrally filtered and detected by a photodiode. Experiments were performed at $T\approx$10 K.

The diamond chip was a chemical-vapor-deposition-grown, single crystal with dimensions 4.5$\times$4.5$\times$0.5 mm^3 and nitrogen density [N]$\lesssim$1 ppm. The sample was irradiated with 2 MeV electrons (dose: 4×10^{16} cm^{-2}) and subsequently annealed at 800° C for several hours. This resulted in [NV$^-$]=25$\pm$15 ppb, as measured by optical spectroscopy [39]. Two opposing (100) sides of the diamond were polished and coated with Ag to produce 80-nm-thick mirrors. On one side, two windows ($\sim$0.5 $\times$ 0.5 mm^2) were left uncoated to permit optical transmission.
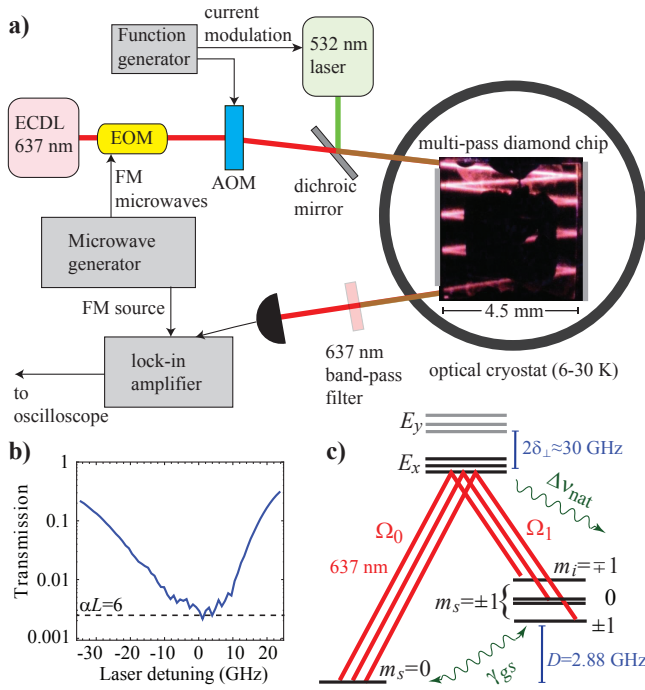
FIG. 1. (a) Experimental apparatus. Microwave frequency modulation (FM) and lock-in detection were used for magnetometry (Fig. 4). AOM–acousto-optic modulator. The dark square on the diamond surface is from a (disconnected) gold electrode. (b) Transmission spectrum of a weak optical probe. (c) NV level structure and allowed Λ transitions at $B = 0$ in the moderate-strain regime. ^{14}N quadrupole splitting is omitted.
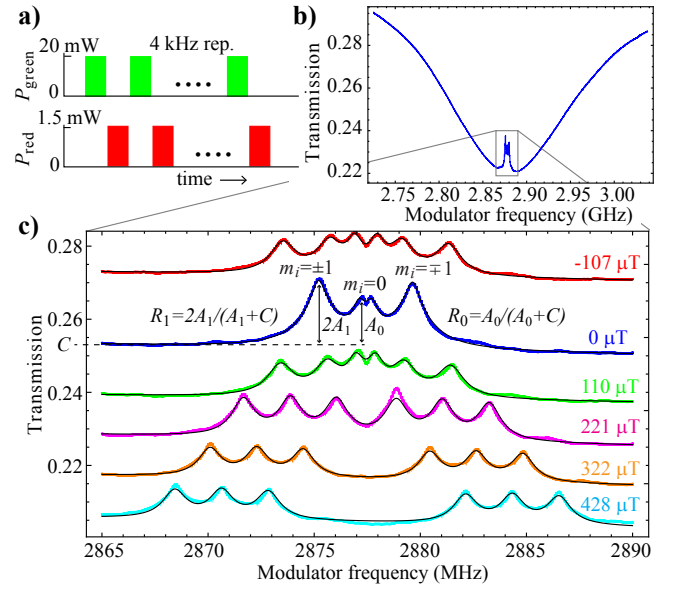

FIG. 2. (a) Timing diagram of optical pulses used to probe EIT resonances. (b) Transmission spectrum as the sideband-carrier detuning was swept through two-photon resonance. (c) EIT spectra at different magnetic fields applied along a [100] direction. The spectra are offset for clarity. Overlayed are Lorentzian fits (see text). In (b,c) $\Delta_L \approx -15$ GHz.

This configuration allowed 8 passes through the diamond, limited by the angular deviation between the polished sides. An optical micrograph of the laser-induced fluorescence is shown within Fig. 1(a). The beam ($\sim$100 μm diameter) was collimated over the entire propagation length. Figure 1(b) shows the zero-phonon line transmission spectrum of a 500 nW probe. The optical depth reaches $\alpha L=6$ with full-width-at-half-maximum (FWHM) $\sim$30 GHz. Throughout, we normalize transmission by its off-resonant, room-temperature value, to account for interface losses, and the laser detuning, Δ_L, is relative to absorption maximum (470.480 THz).

Figure 1(c) illustrates the NV level structure. The center possesses C_{3v} symmetry, with a paramagnetic ($S=1$) ground state and two $S=1$ excited-state orbitals [44, 45]. Under moderate transverse strain, $\delta_\perp$=15$\pm$10 GHz, level anticrossings in the lower excited-state orbital (E_x) mix electron spin projection, permitting optical transitions from both ground-state $m_s=0$ and $m_s=\pm1$ manifolds [36, 38]. The $m_s=0$ and $m_s=\pm1$ manifolds are split at zero magnetic field by D=2.88 GHz, and hyperfine coupling with the ^{14}N nucleus ($I=1$) results in three separate Λ schemes.

Figure 2(a) shows the timing of optical pulses used to

observe EIT. Alternating green and red pulses was necessary to simultaneously achieve high EIT contrast and minimize bleaching. To efficiently excite both arms of the Λ transitions [Fig. 1(c)], the sinusoidal optical phase modulation was set to yield a sideband:carrier:sideband intensity ratio of 0.7:1:0.7 (Supplementary Information, SI). Higher-order sidebands contributed $<$ 8% of the total intensity and are neglected in our analysis.

Figure 2(b) shows the transmitted red light as a function of EOM drive frequency, $\nu_{\rm EOM}$. The broad anti-hole is due to optical pumping [34]. When $|\nu_{\rm EOM}-D| \gg \Delta\nu_{\rm nat}$, where $\Delta\nu_{\rm nat}$=15 MHz [46] is the homogenous excited-state linewidth, NV centers resonant with one of the excitation frequencies can be excited from one spin sublevel, but are eventually trapped in the other sublevel, resulting in high transmission. As $\nu_{\rm EOM}$ approaches 2.88 GHz, one of the sidebands acts as a re-pump for the carrier, so there are no trap states, resulting in lower transmission. The FWHM of this feature (typically 50-200 MHz) depends on several factors, including excited-state dephasing [31], optical power ($P_{\rm red}$), and spectral diffusion [27, 38], but it is always $> \Delta\nu_{\rm nat}$.

As $\nu_{\rm EOM}$ matches exactly the ground-state splitting (two-photon resonance), the transmission increases sharply. These resonances are the hallmark of EIT, and they exhibit much narrower FWHM, $\Delta\nu_{\rm eit}$=0.4-1.3 MHz $\ll \Delta\nu_{\rm nat}$. They occur because NV centers are optically pumped into a "dark" coherent superposition of ground-state levels, $|D\rangle$, which cannot interact with the light due to quantum interference. This

can be understood by considering a simplified model for the NV center consisting of two ground-state levels, $m_s=1$ ($|1\rangle$) and $m_s=0$ ($|0\rangle$) driven optically to a single excited state, $|E_x\rangle$. The Hamiltonian under the rotating wave approximation is:

$$\mathscr{H} = h/(4\pi)(\Omega_0|E_x\rangle\langle 0| + \Omega_1|E_x\rangle\langle 1|) \\ + h(\Delta_1-\Delta_0)|1\rangle\langle 1| + h\Delta_1|E_x\rangle\langle E_x| + h.c., \quad (1)$$

where h is Planck's constant, and Ω_s and Δ_s are, respectively, the Rabi frequency and detuning of the $|s\rangle \leftrightarrow |E_x\rangle$ transition. On two-photon resonance ($\Delta_1=\Delta_2$), the state, $|D\rangle=\frac{1}{\sqrt{\Omega_0^2+\Omega_1^2}}(\Omega_1|0\rangle-\Omega_0|1\rangle)$, is completely decoupled from the optical fields, satisfying $\mathscr{H}|D\rangle=0$. The orthogonal superposition is coupled, so NV centers are pumped into $|D\rangle$, resulting in increased transmission.

The EIT linewidth is limited by the decoherence rate of the dark superposition, γ_{gs}, and its narrow width allows for sensitive, all-optical probing of the NV ground-state level structure. Figure 2(c) shows EIT spectra for several values (B) of magnetic field along a [100] direction. [100]-directed fields preserve the degeneracy of the four NV axes, enabling higher EIT contrast. At $B=0$, the outermost resonances are split by $\sim 2A_{HF}$, where $A_{HF}=-2.17$ MHz is the longitudinal hyperfine coupling constant [47]. The small splitting $\delta_0\approx 0.5$ MHz between the two innermost resonances ($m_i=0$) arises from transverse crystal strain, which behaves as an ensemble-averaged effective electric field [48]. This effective electric field is $|E_\perp|=\delta_0/(2d_{gs_\perp})\approx 15$ kV/cm, where $d_{gs_\perp}=17$ Hz/V/cm is the ground-state transverse dipole moment [49].

The values of $\nu_{\rm EOM}$ on two-photon resonance are approximately equal to the ground-state transition frequencies [50]:

$$\nu_{i_\pm}=D\pm\sqrt{(g\mu_B B\cos\theta + m_i A_{HF})^2 + (d_{gs_\perp}E_\perp)^2}, \quad (2)$$

where $g=2.003$ is the electron-spin g-factor [51], $\mu_B=13.996$ GHz/T is the Bohr magneton, and $\cos\theta\approx 1/\sqrt{3}$ is the projection of the field along each NV axis. Equation (2) neglects AC Stark shifts of order $\Omega_0^2/(16\pi^2\Delta_e)\lesssim 10$ kHz, where $\Delta_e\approx 0.5$ GHz is a typical frequency separation between excited states (SI).

We fit the spectra to a sum of six Lorentzian profiles (plus an offset C), with amplitude A, and FWHM $\Delta\nu_{\rm eit}$. The central frequencies were constrained by Eq. (2); D and $E_\perp$ were fit globally, while B, $\Delta\nu_{\rm eit}$, A, and C were allowed to vary between spectra. Resonances that satisfied $|g\mu_B B\cos\theta + m_i A_{HF}| < d_{gs_\perp}|E_\perp|$ (innermost resonances within the top three spectra in Fig. 2) were given separate amplitude (A_0) and FWHM ($\Delta\nu_{\rm eit,0}$) from those where the condition was not held (A_1, $\Delta\nu_{\rm eit,1}$) [50].

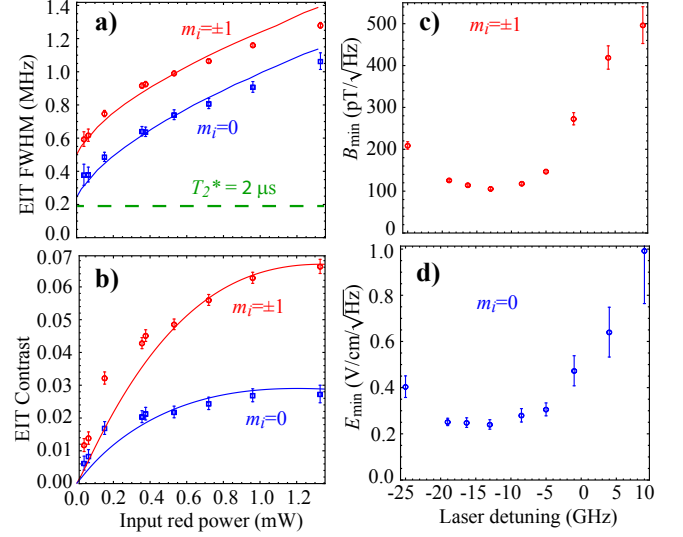To gain further insight into the EIT lineshapes, we determined the contrast and FWHM as a function of

FIG. 3. (a,b) Power dependence of zero-field EIT FWHM and contrast ($\Delta_L\approx -13$ GHz) determined from Lorentzian fits as in Fig. 2(c). (c,d) Photon-shot-noise-limited magnetic and electric field sensitivity [Eq. (3)], inferred from zero-field EIT spectra, as a function of laser detuning.

$P_{\rm red}$ at $B=0$, Fig. 3(a,b). For $m_i=0$ resonances, the zero-field contrast is here defined as $R_0=A_0/(A_0 + C)$, and for $m_i=\pm 1$ resonances it is $R_1=2A_1/(A_1 + C)$. These data were fit by a 3-level density-matrix model for EIT in inhomogenously-broadened media (SI) [34]. The fit parameters include a Rabi frequency conversion factor, $P_{\rm sat}\equiv\pi\Delta\nu_{\rm nat}^2 P_{\rm red}/\Omega_0^2=2.4\pm 1.1$ mW, the ratio $\Omega_1/\Omega_0=0.08\pm 0.02$, which reflects the ensemble-averaged asymmetry in Λ transition strengths [38], and nuclear-spin-dependent ground-state dephasing [50] $\gamma_{gs,m_i=\pm 1}/(2\pi)=240\pm 92$ kHz and $\gamma_{gs,m_i=0}/(2\pi)=99\pm 30$ kHz. The apparent saturation of the contrast arises from photo-ionization (SI), which reduces [NV⁻] at a rate $\propto P_{\rm red}^2$ [43]. Above $T\approx 10$ K, the contrast falls off sharply with temperature, becoming negligible at $T\approx 30$ K. This effect (SI) is well described by a nine-level model of the NV center that includes temperature-dependent excited-state dephasing [31].

Near $B\approx 0$, the EIT resonances provide a means to simultaneously sense electric and magnetic fields. The theoretical sensitivity of an electric or magnetic field sensor based on an optically-detected signal, S, is given by the minimum detectable field which gives signal:noise=1; $\delta E_{min}=\frac{\delta S}{|dS/dE|}$ and $\delta B_{min}=\frac{\delta S}{|dS/dB|}$, where δS is the standard deviation of S [52]. From Eq. (2), we see that $dS/dE\approx 0$ except when $|g\mu_B B + m_i A_{HF}|\lesssim d_{gs_\perp}|E_\perp|$. At $B\approx 0$, this condition is satisfied for the $m_i=0$ resonances, whereas high-sensitivity magnetometry is possible using the $m_i=\pm 1$ resonances provided $|E_\perp|\lesssim|A_{HF}|/d_{gs_\perp}\approx 130$ kV/cm.

If δS is limited by photon shot noise, the magnetic

sensitivity is (SI):

$$\delta B_{min} \simeq \frac{1}{g\mu_B \cos\theta} \frac{\Delta\nu_{\text{eit}}}{R_1} \sqrt{\frac{E_p}{Pt_m}}, \qquad (3)$$

where P is the detected optical power, E_p is the photon energy, and t_m is the measurement time. A similar expression can be found for sensitivity to electric fields within diamond (SI), substituting $d_{gs_\perp}R_0$ for $g\mu_B R_1$ [50] (neglecting crystal-strain inhomogeneity). These equations assume detected fields lie along a [100] direction, but arbitrarily-oriented fields can be detected using a suitable bias field [53, 54].

We studied the projected electrometer and magnetometer performance by analyzing zero-field EIT spectra as a function of Δ_L, Fig. 3(c-d). In both cases, the sensitivity is optimized in the range $\Delta_L = -5$ to -20 GHz. Not surprisingly, this corresponds to the range of $|E_x\rangle$ strain shifts where Λ transitions have been observed in single-NV experiments [38]. The optimal sensitivities ($\Delta_L = -13$ GHz) are 105 ± 6 pT/$\sqrt{\text{Hz}}$ and 0.24 ± 0.04 V/cm/$\sqrt{\text{Hz}}$ for magnetometry and electrometry, respectively. Throughout we use the metrology convention that 1 Hz measurement bandwidth corresponds to $t_m = 0.5$ s.

High-sensitivity operation of our device as an all-optical magnetometer was accomplished using lock-in detection of a resonance peak [55] in a bias field $B = 0.2$ mT [Fig. 4(a)]. A microwave signal $\nu_{\text{EOM}} = 2.8717$ GHz was frequency-modulated at 89 kHz [56], with deviation 300 kHz$_{\text{pp}}$, and sent to the EOM. The photodetector signal was demodulated using a lock-in amplifier, and the in-phase signal was sent to an oscilloscope. Figure 4(b) shows the magnetometer response when a separately-calibrated test field was applied. Additional calibrations are presented in SI. Summarizing, the magnetometer response remains linear over a range of $\gtrsim 1$ μT, and the bandwidth covers ~ 100 Hz (limited here by electronic filtering).

To characterize the sensitivity, the magnetic noise was measured without a test field. Figure 4(c) shows the noise-equivalent magnetic field spectrum. The noise floor is $\lesssim 1$ nT/$\sqrt{\text{Hz}}$ for frequencies above 10 Hz. The floor was dominated by lock-in amplifier input noise, as evidenced by its persistence when the photodetector was unplugged. The expected shot noise, based on Eq. (3) after incorporating the finite quantum efficiency of the detector, is 0.3 nT/$\sqrt{\text{Hz}}$.

Near 1 Hz, the noise floor rises. A possible cause is instabilities in P_{red} lead to fluctuations in AC Stark shifts (SI). Nevertheless, the magnetometer recovers high sensitivity for long integration times, as evidenced by the Allan deviation [47] plotted in Fig. 4(d). For a gate time of 100 s, the Allan deviation is 1.3 ± 1.1 nT.

In comparing with existing technologies, we are not aware of another sensor that simultaneously measures low-frequency electric and magnetic fields with high sensitivity. Miniature vapor-cell magnetometers [57]
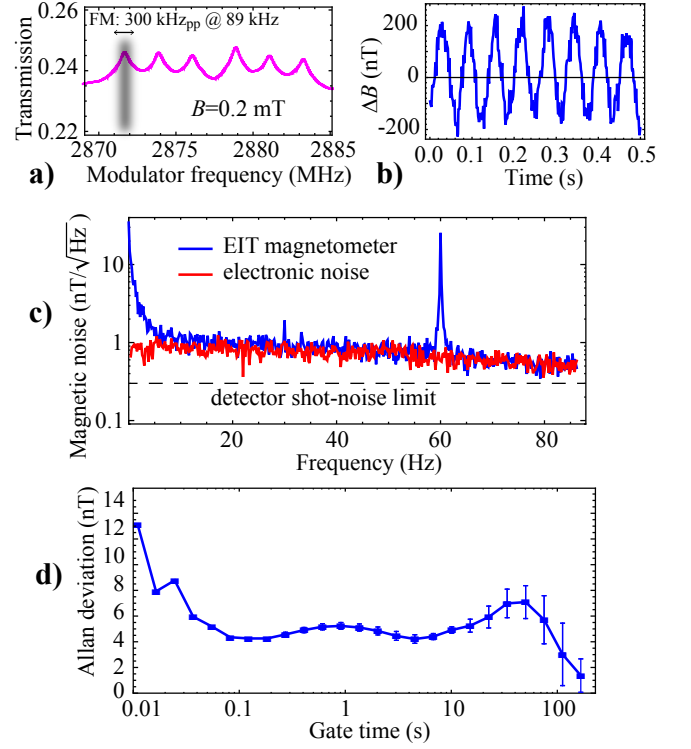

FIG. 4. (a) Schematic of the frequency modulation (FM) technique employed for magnetometry. (b) Lock-in signal when a 16-Hz oscillating field (350 nT$_{\text{PP}}$) was applied along a [100] direction. (c) Magnetic noise spectrum of the EIT magnetometer. The spike at 60 Hz is a real magnetic signal arising due to operation in an unshielded environment (SI). Also shown is the noise spectrum when the photodetector was unplugged. (d) Allan deviation of a 500 s data set.

achieve low-frequency sensitivity of ~ 0.01 pT/$\sqrt{\text{Hz}}$ at $T \approx 470$ K, but the sensitivity rapidly degrades with decreasing temperature [52]. At low temperature, miniature superconducting quantum interference devices have excellent sensitivity, $\delta B_{min} \lesssim 0.1$ pT/$\sqrt{\text{Hz}}$. However they typically suffer from $1/f$ noise, so DC measurements require external calibration [58]. In addition to its long-term stability and dual electric/magnetic field sensitivity, our sensor is probed entirely optically, in large electric fields, and it does not produce fields of its own.

Future applications may benefit from several improvements. Higher EIT contrast is possible using spectral filtering to detect only one optical frequency, tailoring the absorption spectrum using holeburning techniques [59], or employing other magnetic/electric field geometries [33, 38]. The coherence time can be extended by orders of magnitude using dynamic decoupling [30] and/or with isotopically-pure diamond [47, 60, 61]. Finally, integration with optical cavities [26, 28, 29] will allow higher optical depth and larger optical intensities, while decreasing the device volume.

In summary, we observed narrow EIT resonances in a multi-pass diamond chip. The high optical depth and

narrow inhomogenous linewidth enable new diamond-based applications including all-optical electrometry and magnetometry. We operated a prototype diamond-EIT magnetometer with sub-nT/$\sqrt{\text{Hz}}$ sensitivity and excellent long-term stability. Integration with photonic networks may enable new applications, including few-photon nonlinear optics and quantum-optical memories.

---

* victor.acosta@hp.com; Equal contribution
† kasperjensen@berkeley.edu; Equal contribution

[1] S. Brandt, A. Nagel, R. Wynands, and D. Meschede, Physical Review A **56**, R1063 (1997).

[2] D. Budker, D. Kimball, S. Rochester, and V. Yashchuk, Physical Review Letters **83**, 1767 (1999).

[3] M. Klein, I. Novikova, D. F. Phillips, and R. L. Walsworth, Journal of Modern Optics **53**, 2583 (2006).

[4] R. Röhlsberger, H.-C. Wille, K. Schlage, and B. Sahoo, Nature **482**, 199 (2012).

[5] L. V. Hau, S. E. Harris, Z. Dutton, and C. H. Behroozi, Nature **397**, 594 (1999).

[6] A. Nagel, L. Graf, and A. Naumov, Europhysics Letters **31** (2007).

[7] J. Vanier, Applied Physics B **81**, 421 (2005).

[8] R. Santra, E. Arimondo, T. Ido, C. Greene, and J. Ye, Physical Review Letters **94**, 173002 (2005).

[9] V. I. Yudin, A. V. Taichenachev, Y. O. Dudin, V. L. Velichansky, A. S. Zibrov, and S. A. Zibrov, Physical Review A **82**, 033807 (2010).

[10] S. Harris and L. Hau, Physical Review Letters **82**, 4611 (1999).

[11] M. Bajcsy, S. Hofferberth, V. Balic, T. Peyronel, M. Hafezi, A. Zibrov, V. Vuletic, and M. Lukin, Physical Review Letters **102**, 203902 (2009).

[12] M. Albert, A. Dantan, and M. Drewsen, Nature Photonics **5**, 633 (2011).

[13] T. Peyronel, O. Firstenberg, Q.-Y. Liang, S. Hofferberth, A. V. Gorshkov, T. Pohl, M. D. Lukin, and V. Vuletić, Nature **488**, 57 (2012).

[14] A. Kasapi, M. Jain, G. Yin, and S. Harris, Physical Review Letters **74**, 2447 (1995).

[15] J. B. Khurgin, Journal of the Optical Society of America B **22**, 1062 (2005).

[16] R. Boyd, D. Gauthier, A. Gaeta, and A. Willner, Physical Review A **71**, 023801 (2005).

[17] A. I. Lvovsky, B. C. Sanders, and W. Tittel, Nature Photonics **3**, 706 (2009).

[18] W. Tittel, M. Afzelius, T. Chaneliére, R. Cone, S. Kröll, S. Moiseev, and M. Sellars, Laser & Photonics Reviews **4**, 244 (2009).

[19] I. Novikova, R. Walsworth, and Y. Xiao, Laser & Photonics Reviews **6**, 333 (2012).

[20] A. Gorshkov, A. André, M. Fleischhauer, A. Sørensen, and M. Lukin, Physical Review Letters **98**, 123601 (2007).

[21] B. S. Ham, P. R. Hemmer, and M. S. Shahriar, Optics Communications **144**, 227 (1997).

[22] P. Goldner, O. Guillot-Noël, F. Beaudoux, Y. Le Du, J. Lejay, T. Chanelière, J.-L. Le Gouët, L. Rippe, A. Amari, A. Walther, and S. Kröll, Physical Review A **79**, 033809 (2009).

[23] E. Baldit, K. Bencheikh, P. Monnier, S. Briaudeau, J. A. Levenson, V. Crozatier, I. Lorgeré, F. Bretenaker, J. L. Le Gouët, O. Guillot-Noël, and P. Goldner, Physical Review B **81**, 144303 (2010).

[24] G. Davies and M. F. Hamer, Proceedings of the Royal Society A: Mathematical, Physical and Engineering Sciences **348**, 285 (1976).

[25] B. B. Buckley, G. D. Fuchs, L. C. Bassett, and D. D. Awschalom, Science **330**, 1212 (2010).

[26] I. Aharonovich and A. Greentree, Nature Photonics **5**, 397 (2011).

[27] A. Faraon, C. Santori, Z. Huang, V. M. Acosta, and R. G. Beausoleil, Physical Review Letters **109**, 033604 (2012).

[28] B. J. M. Hausmann, B. Shields, Q. Quan, P. Maletinsky, M. McCutcheon, J. T. Choy, T. M. Babinec, A. Kubanek, A. Yacoby, M. D. Lukin, and M. Loncar, Nano letters (2012).

[29] A. Faraon, C. Santori, Z. Huang, K.-M. C. Fu, V. M. Acosta, D. Fattal, and R. G. Beausoleil, New Journal of Physics **15**, 025010 (2013).

[30] N. Bar-Gill, L. M. Pham, A. Jarmola, D. Budker, and R. L. Walsworth, (2012), arXiv:1211.7094.

[31] K.-M. C. Fu, C. Santori, P. E. Barclay, L. J. Rogers, N. B. Manson, and R. G. Beausoleil, Physical Review Letters **103**, 256404 (2009).

[32] A. Jarmola, V. M. Acosta, K. Jensen, S. Chemerisov, and D. Budker, Physical Review Letters **108**, 197601 (2012).

[33] P. R. Hemmer, A. V. Turukhin, M. S. Shahriar, and J. A. Musser, Optics Letters **26**, 361 (2001).

[34] C. Santori, D. Fattal, S. M. Spillane, M. Fiorentino, R. G. Beausoleil, A. D. Greentree, P. Olivero, M. Draganski, J. R. Rabeau, P. Reichart, B. C. Gibson, S. Rubanov, D. N. Jamieson, and S. Prawer, Optics Express **14**, 7986 (2006).

[35] C. Santori, P. Tamarat, P. Neumann, J. Wrachtrup, D. Fattal, R. G. Beausoleil, J. Rabeau, P. Olivero, A. D. Greentree, S. Prawer, F. Jelezko, and P. Hemmer, Physical Review Letters **97**, 247401 (2006).

[36] P. Tamarat, N. B. Manson, J. P. Harrison, R. L. McMurtrie, A. Nizovtsev, C. Santori, R. G. Beausoleil, P. Neumann, T. Gaebel, F. Jelezko, P. Hemmer, and J. Wrachtrup, New Journal of Physics **10**, 045004 (2008).

[37] E. Togan, Y. Chu, A. Imamoglu, and M. D. Lukin, Nature **478**, 497 (2011).

[38] V. Acosta, C. Santori, A. Faraon, Z. Huang, K.-M. Fu, A. Stacey, D. Simpson, K. Ganesan, S. Tomljenovic-Hanic, A. Greentree, S. Prawer, and R. Beausoleil, Physical Review Letters **108** (2012).

[39] V. M. Acosta, E. Bauch, M. P. Ledbetter, C. Santori, K. M. C. Fu, P. E. Barclay, R. G. Beausoleil, H. Linget, J. F. Roch, F. Treussart, S. Chemerisov, W. Gawlik, and D. Budker, Physical Review B **80**, 115202 (2009).

[40] I. Altarev, C. Baker, G. Ban, G. Bison, K. Bodek,

M. Daum, P. Fierlinger, P. Geltenbort, K. Green, M. van der Grinten, E. Gutsmiedl, P. Harris, W. Heil, R. Henneck, M. Horras, P. Iaydjiev, S. Ivanov, N. Khomutov, K. Kirch, S. Kistryn, A. Knecht, P. Knowles, A. Kozela, F. Kuchler, M. Kuźniak, T. Lauer, B. Lauss, T. Lefort, A. Mtchedlishvili, O. Naviliat-Cuncic, A. Pazgalev, J. Pendlebury, G. Petzoldt, E. Pierre, G. Pignol, G. Quéméner, M. Rebetez, D. Rebreyend, S. Roccia, G. Rogel, N. Severijns, D. Shiers, Y. Sobolev, A. Weis, J. Zejma, and G. Zsigmond, Physical Review Letters **103**, 081602 (2009).

[41] D. H. Beck, D. Budker, B. K. Park, and N. Collaboration, Il Nuovo Cimento C **35**, 116 (2012).

[42] L.-S. Bouchard, V. M. Acosta, E. Bauch, and D. Budker, New Journal of Physics **13**, 025017 (2011).

[43] N. Aslam, G. Waldherr, P. Neumann, F. Jelezko, and J. Wrachtrup, New Journal of Physics **15**, 013064 (2013).

[44] J. Maze, A. Gali, E. Togan, Y. Chu, A. S. Trifonov, E. Kaxiras, and M. D. Lukin, New Journal of Physics **13**, 25025 (2011).

[45] M. W. Doherty, N. B. Manson, P. Delaney, and L. C. L. Hollenberg, New Journal of Physics **13**, 25019 (2011).

[46] A. Batalov, C. Zierl, T. Gaebel, P. Neumann, I. Y. Chan, G. Balasubramanian, P. R. Hemmer, F. Jelezko, and J. Wrachtrup, Physical Review Letters **100**, 77401 (2008).

[47] K. Fang, V. M. Acosta, C. Santori, Z. Huang, K. M. Itoh, H. Watanabe, S. Shikata, and R. G. Beausoleil, (2012), arXiv:1212.1495.

[48] A. E. Hughes and W. A. Runciman, Proceedings of the Physical Society **90**, 827 (1967).

[49] E. van Oort and M. Glasbeek, Chemical Physics Letters **168**, 529 (1990).

[50] F. Dolde, H. Fedder, M. W. Doherty, T. Nöbauer, F. Rempp, G. Balasubramanian, T. Wolf, F. Reinhard, L. C. L. Hollenberg, F. Jelezko, and J. Wrachtrup, Nature Physics **7**, 459 (2011).

[51] S. Felton, A. M. Edmonds, M. E. Newton, P. M. Martineau, D. Fisher, D. J. Twitchen, and J. M. Baker, Physical Review B (Condensed Matter and Materials Physics) **79**, 75203 (2009).

[52] D. Budker and M. Romalis, Nature Physics **3**, 227 (2007).

[53] J. M. Taylor, P. Cappellaro, L. Childress, L. Jiang, D. Budker, P. R. Hemmer, A. Yacoby, R. Walsworth, and M. D. Lukin, Nature Physics **4**, 810 (2008).

[54] B. J. Maertz, A. P. Wijnheijmer, G. D. Fuchs, M. E. Nowakowski, and D. D. Awschalom, Applied Physics Letters **96**, 92503 (2010).

[55] V. M. Acosta, E. Bauch, A. Jarmola, L. J. Zipp, M. P. Ledbetter, and D. Budker, Applied Physics Letters **97**, 174104 (2010).

[56] C. S. Shin, C. E. Avalos, M. C. Butler, D. R. Trease, S. J. Seltzer, J. Peter Mustonen, D. J. Kennedy, V. M. Acosta, D. Budker, A. Pines, and V. S. Bajaj, Journal of Applied Physics **112**, 124519 (2012).

[57] W. C. Griffith, S. Knappe, and J. Kitching, Optics Express **18**, 27167 (2010).

[58] J. Clarke and A. I. Braginski, *The SQUID Handbook* (Wiley-VCH, 2006).

[59] N. R. S. Reddy, N. B. Manson, and E. R. Krausz, Journal of Luminescence **38**, 46 (1987).

[60] G. Balasubramanian, P. Neumann, D. Twitchen, M. Markham, R. Kolesov, N. Mizuochi, J. Isoya, J. Achard, J. Beck, J. Tissler, V. Jacques, P. R. Hemmer, F. Jelezko, and J. Wrachtrup, Nat Mater **8**, 383 (2009).

[61] T. Ishikawa, K.-M. C. Fu, C. Santori, V. M. Acosta, R. G. Beausoleil, H. Watanabe, S. Shikata, and K. M. Itoh, Nano letters **12**, 2083 (2012).